WAVE PROPAGATION ANALYSIS WITH ADAPTIVE TIME INTEGRATION PARAMETERS

Delfim Soares Júnior

Danielle R de Medeiros Leal

delfim.soares@ufjf.edu.br

danielle.leal@engenharia.ufjf.br

Faculty of Engineering, Federal University of Juiz de Fora

Cidade Universitária, CEP 36036-330, Juiz de Fora, MG, Brazil.

Abstract. *In this work, a new explicit time-marching technique is presented for wave propagation analysis, which is based on adaptive time integrators. In this novel approach, the properties of the time integration methodology are modified at each time-step, according to the computed solution. Thus, numerical damping can be locally and adaptively introduced, allowing spurious modes to be properly eliminated without significantly affecting the accuracy of the main modes of the model. In addition, multiple time-steps are adaptively computed, according to the local properties of the model, ensuring stability and efficiency to the explicit analysis in focus. The technique is direct (i.e., non-iterative) and very effective: the renew of the time integration parameters is evaluated once for each time-step and independently for each spatial discretization subdomain (local attribution), enabling specific features to be activated locally along time and space. At the end of the paper, numerical results are presented, illustrating the performance and potentialities of the proposed approach.*

Keywords: *Time Integration Methods, Wave Propagation, Adaptive Dissipation Control, Subcycling, Finite Element Method.*

1 INTRODUCTION

Wave propagation problems, considering time-domain analysis, require advanced techniques for spatial and temporal discretization (Soares, 2014a, 2015; Groβeholz et al., 2015). In this context, this work discusses a adaptive time marching procedure for hyperbolic models, which is explicit and requires no system of equations to be dealt with. The method is conditionally-stable, truly self-starting and presents controllable numerical dissipation, which adapts locally and at each time-step, according to the computed solution. Its adaptive algorithmic dissipation is based on a simple local oscillatory criterion (Soares, 2014b). Due to the conditional stability of the explicit approach, the use of multiple time-steps is recommended, in order to improve the performance to the method. In this context, subcycling is employed here. Thus, various time-steps are considered, which are adaptively computed according to the physical and geometrical properties of the model. Since different time-steps are considered, interpolations of the solutions are required and the adoption of multiple time increments provides a more robust algorithm.

The paper is organized as follows: first, the governing equations of the model and the time integration strategy are presented, describing the basic aspects and the adaptive features of the formulation. In the sequence, the properties of the method are discussed, and the adopted subcycling technique is presented, describing the proposed methodology. At the end of the manuscript, a numerical application is considered, illustrating the good performance of the novel approach.

2 GOVERNING EQUATIONS

The hyperbolic model in focus is described by:

$$\mathbf{M}\ddot{\mathbf{U}}(t) + \mathbf{K}\mathbf{U}(t) = \mathbf{F}(t) \tag{1}$$

where $\mathbf{M}$ and $\mathbf{K}$ stand for matrices and $\mathbf{F}(t)$ and $\mathbf{U}(t)$ stand for vectors (overdots symbolize time derivatives). The initial conditions of the model are given by $\mathbf{U}^0 = \mathbf{U}(0)$ and $\dot{\mathbf{U}}^0 = \dot{\mathbf{U}}(0)$.

Writing Eq. (1) in an integral form, at the element level (element variables are indicated by subscript e), considering a time-step Δt, the following expression is obtained:

$$\mathbf{M}_e \int_{t-\frac{\Delta t}{2}}^{t+\frac{\Delta t}{2}} \ddot{\mathbf{U}}_e(\tau) d\tau + \mathbf{K}_e \int_{t-\frac{\Delta t}{2}}^{t+\frac{\Delta t}{2}} \mathbf{U}_e(\tau) d\tau = \int_{t-\frac{\Delta t}{2}}^{t+\frac{\Delta t}{2}} \mathbf{F}_e(\tau) d\tau \tag{2}$$

The integrals in the l.h.s. of Eq.(2) may be computed as:

$$\Im_{\ddot{\mathbf{U}}_e}^{n+\frac{1}{2}} = \int_{t-\frac{\Delta t}{2}}^{t+\frac{\Delta t}{2}} \ddot{\mathbf{U}}_e(\tau) d\tau \approx \dot{\mathbf{U}}_e^{n+1} - \dot{\mathbf{U}}_e^{n} \tag{3a}$$

$$\mathfrak{I}_{\mathbf{U}_e}^{n+\frac{1}{2}} = \int_{t-\frac{\Delta t}{2}}^{t+\frac{\Delta t}{2}} \mathbf{U}_e(\tau) d\tau \approx \Delta t\, \mathbf{U}_e^n + \tfrac{1}{2}\alpha_e^n \Delta t^2 \dot{\mathbf{U}}_e^n \tag{3b}$$

where $\mathbf{U}^n$ and $\dot{\mathbf{U}}^n$ are approximations of $\mathbf{U}(t^n)$ and $\dot{\mathbf{U}}(t^n)$, respectively, $t^n = n\Delta t$ and α_e^n is the time integration parameter used in the adopted integration strategy, which is evaluated at each time-step and at each element.

Using the approximations described in Eqs. (3), Eq. (2) may be rewritten as:

$$\mathbf{M}_e\, \dot{\mathbf{U}}_e^{n+1} = \mathfrak{I}_{\mathbf{F}_e}^{n+\frac{1}{2}} + \mathbf{M}_e \dot{\mathbf{U}}_e^n - \mathbf{K}_e(\Delta t \mathbf{U}_e^n + \tfrac{1}{2}\alpha_e^n \Delta t^2 \dot{\mathbf{U}}_e^n) \tag{4}$$

which, in conjunction with the following simple finite difference expression:

$$\mathbf{U}^{n+1} = \mathbf{U}^n + \tfrac{1}{2}\Delta t \dot{\mathbf{U}}^n + \tfrac{1}{2}\Delta t \dot{\mathbf{U}}^{n+1} \tag{5}$$

define the recursive relationship of the present methodology.

As one may note, once $\mathbf{M}$ is modeled as a diagonal matrix, no system of equations has to be dealt with after assembling is considered. Eq. (4) and Eq. (5) allow to compute $\dot{\mathbf{U}}^{n+1}$ and $\mathbf{U}^{n+1}$, respectively, at the current time-step. As it can be observed, the method does not employ the vector $\ddot{\mathbf{U}}^{n+1}$ in its formulation, which makes it truly self-starting, eliminating possible cumbersome initial procedures, such as the computation of $\ddot{\mathbf{U}}^0$ or multistep initial values.

As previously remarked, the α parameter is computed at each time-step and at each element. This is carried out based on an oscillatory criterion, which takes into account the results at the last three time-steps, as described in Eqs. (6). Thus, if the computed response of a degree of freedom oscillates along time, the α parameters of the elements surrounding this degree of freedom are modified, locally introducing numerical dissipation. Once no oscillatory behavior is observed, this parameter is kept unitary.

$$\varphi_e^n = \sum_{i=1}^{\eta_e} \left(\left| u_i^n - u_i^{n-2} \right| - \left| u_i^n - u_i^{n-1} \right| - \left| u_i^{n-1} - u_i^{n-2} \right| \right) \tag{6a}$$

$$\text{if } \varphi_e^n = 0, \alpha_e^n = 1 \tag{6b}$$

$$\text{if } \varphi_e^n \neq 0, \alpha_e^n = \frac{4}{\omega_e \Delta t} - 1 \tag{6c}$$

In Eqs. (6), η_e stands for the total amount of degrees of freedom of the element, and ω_e stands as its maximal natural frequency. In next section, the properties of the technique are analyzed.

3 PROPERTIES OF THE METHOD

In this section, a single degree of freedom (SDOF) problem, as described in Eq. (7), is considered in order to discuss the properties (e.g., stability, accuracy etc.) of the method.

$$\ddot{u}(t)+w^2u(t)=f(t) \tag{7}$$

In Eq. (7), w is the natural frequency of the model. Considering the proposed methodology, the following recursive relationship can be written:

$$\begin{bmatrix} u^{n+1} \\ \dot{u}^{n+1} \end{bmatrix} = \begin{bmatrix} A_{11} & A_{12} \\ A_{21} & A_{22} \end{bmatrix} \begin{bmatrix} u^{n} \\ \dot{u}^{n} \end{bmatrix} + \begin{bmatrix} L_{11} & L_{12} & L_{13} \\ L_{21} & L_{22} & L_{23} \end{bmatrix} \begin{bmatrix} f^{n} \\ f^{n+\frac{1}{2}} \\ f^{n+1} \end{bmatrix} = \mathbf{A} \begin{bmatrix} u^{n} \\ \dot{u}^{n} \end{bmatrix} + \mathbf{L} \begin{bmatrix} f^{n} \\ f^{n+\frac{1}{2}} \\ f^{n+1} \end{bmatrix} \tag{8}$$

where **A** and **L** are the amplification and the load operator matrices, respectively, which are given by:

$$\mathbf{A} = \begin{bmatrix} 1-\frac{1}{2}w^2\Delta t^2 & \left(1-\frac{1}{4}\alpha w^2\Delta t^2\right)\Delta t \\ -w^2\Delta t & 1-\frac{1}{2}\alpha w^2\Delta t^2 \end{bmatrix} \tag{9}$$

$$\mathbf{L} = \begin{bmatrix} \frac{1}{2}\beta_1\Delta t^2 & \frac{1}{2}\beta_2\Delta t^2 & \frac{1}{2}\beta_3\Delta t^2 \\ \beta_1\Delta t & \beta_2\Delta t & \beta_3\Delta t \end{bmatrix} \tag{10}$$

In Eq. (10), β_1, β_2 and β_3 are the load integration parameters, which can be selected, for instance, as $\beta_1=\beta_3=1/4$ and $\beta_2=1/2$, if the trapezoidal rule is followed, or as $\beta_1=\beta_3=1/6$ and $\beta_2=2/3$, if the Simpson rule is followed. If linear behavior is assumed for the load within Δt, the load integration parameters can be simply selected as $\beta_1=\beta_3=1/2$ and $\beta_2=0$. As it can be inferred from Eq. (9), the method is second-order accurate for $\alpha=1$, and first order accurate otherwise.

3.1 Stability and numerical dissipation

To assure the stability of the method, the spectral radius of matrix A (which represents the maximal absolute magnitude of the eigenvalues of A) should not be greater than 1(Bathe, 1996; Hughes, 2000). In the present technique, the eigenvalues of A are defined by:

$$\lambda_{1,2}(\mathbf{A}) = A_1 \pm (A_1^2 - A_2)^{1/2} \tag{11a}$$

$$A_1 = \left[1 - (1/4)(\alpha+1)\Omega^2\right] \tag{11b}$$

$$A_2 = \left[1 + (1/2)(1-\alpha)\Omega^2\right] \tag{11c}$$

where $\Omega = w\Delta t$ is the sampling frequency of the model.

The method is conditionally stable for $\alpha \geq 1$ and unconditionally unstable for $\alpha < 1$. Once $\alpha = 1$, no numerical damping is introduced into the algorithm and the main features of the Central Difference Method (CDM) are reproduced. If $\alpha > 1$, numerical dissipation is considered. Because the higher modes of semidiscrete equations are artifacts of the discretization process and not representative of the behaviour of the governing partial differential equations, it is generally viewed as desirable and often is considered absolutely necessary to have some form of algorithmic damping present to remove the participation of the high-frequency modal components (Hughes, 2000).

The value of Ω under which the stability of the method is assured, is given by (critical sampling frequency):

$$\Omega_C = 2\alpha^{-1/2} \tag{14}$$

The value of Ω in which complex eigenvalues bifurcate into real and distinct values, is given by (bifurcation sampling frequency):

$$\Omega_B = 4(\alpha+1)^{-1} \tag{15}$$

Thus, considering expression (6c), the bifurcation sampling frequency equals the maximal sampling frequency of the element. The spectral radius reaches its minimal value at the bifurcation sampling frequency. In this case, $\rho_B = |\alpha - 3|/|\alpha + 1|$. Therefore, if $\alpha = 3$, $\rho_B = 0$ and $\Omega_B = 1$. In Fig. 1(a), a scheme illustrating the main characteristics of the spectral radius as function of α is presented and, in Fig.1(b), some curves for the spectral radii are depicted.

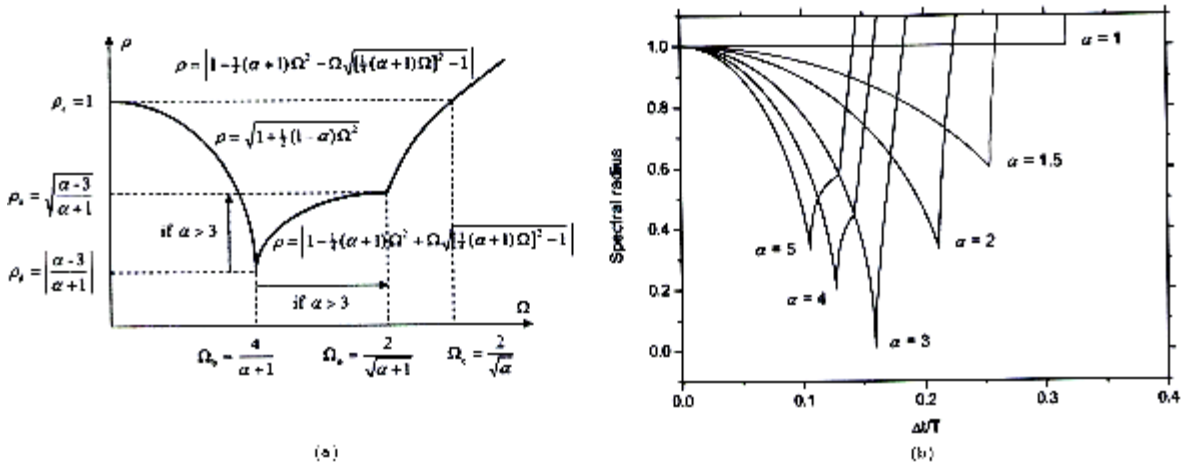

Figure 1. (a) Spectral radius behavior; (b) spectral radii.

3.2 Accuracy

As described in Soares (2014c), the accuracy of a hyperbolic time marching technique can be quantified by period elongation, amplitude decay and amplitude factor error measures, which are depicted in Fig.2 for the method in focus, taking into account several values for α .

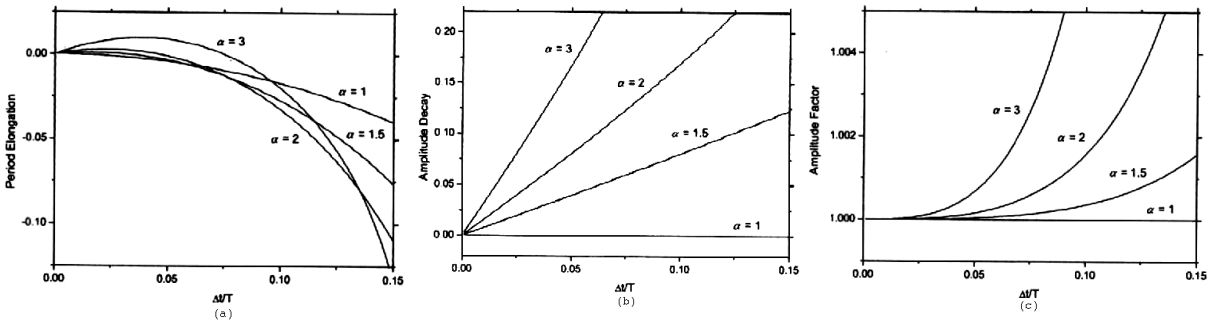

Figure 2. (a) Period elongation; (b) amplitude decay and (c) amplitude factor.

4 SUBCYCLING

Subcycling is an usual approach (Belytschko et al., 1977; Dokainish et al., 1989; etc.), which consists in dividing the global domain in subdomains, each one with an appropriated time-step to be used in the time integration.

The division of the domain considers the critical time-step of the elements. Here, the basic time-step of the analysis (Δt_O) is computed taking into account the element with the highest natural frequency in the model; then, subdomains are created, considering powers of 2 of this basic time-step, in accordance to the stability limit of each region. Thus, each node of the model can be classified in a subdomain, marching in time with its respective time-step. In Fig. 3, an example of a domain subdivision is illustrated, considering an irregular mesh and two time-steps attributions.

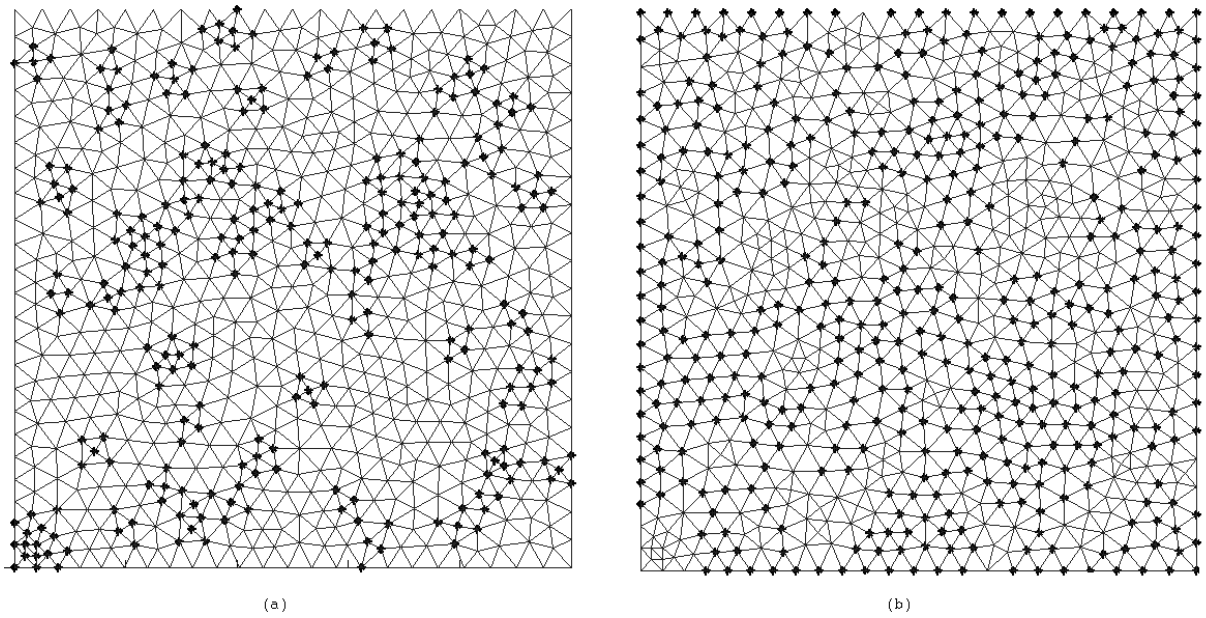

Figure 3. Example of a domain subdivision for the subcycling: (a) nodes in subdomain 1 with $\Delta t_1 = \Delta t_O$; (b) nodes in subdomain 2 with $\Delta t_2 = 2\Delta t_O$.

The solution for each subdomain is computed considering its previous time-step solution (taking into account interpolated values at the border of the subdomains, whenever it is necessary) and the global solution is constructed.

5 NUMERICAL RESULTS

In this section, a numerical example considering electromagnetic wave propagation illustrates the performance of the proposed adaptive technique. Here, electric current densities, flowing in the z-direction, are spatially distributed in square regions (defined by side length l = 0.04L) that are sparsely and anti-symmetrically located over the xy plane, as indicated in Fig. 4. In this figure, the adopted discretized domain is also depicted, which is characterized by a square region with side length 0.5L. The electric currents have Heaviside time behaviour, i.e., they are suddenly applied and kept constant along time. The geometry of the problem is defined by $L = 10\,m$ and the physical properties of the medium (air) are $\mu = 1.2566 \times 10^{-6}\,H/m$ and $\varepsilon = 8.8544 \times 10^{-12}\,F/m$. The model is discretized by 34424 linear triangular finite elements and $\Delta t_O = 2.2851 \times 10^{-11}\,s$.

For this configuration, analytical answers are available and they are expressed by ($0 \le x \le L$ and $0 \le y \le L$):

$$\mathbf{E}(x,y,t) = \frac{4aL}{c\pi^3} \cdot \sum_{m=1}^{\infty}\sum_{n=1}^{\infty}\left[\frac{C_{mn}}{mn(m^2+n^2)^{1/2}} \sin\left(\frac{m}{L}\pi x\right)\sin\left(\frac{n}{L}\pi y\right)\sin\left(\frac{(m^2+n^2)^{1/2}}{L}\pi c t\right)\right]\cdot \mathbf{z} \qquad (16)$$

where $C_{mn} = [\cos(c_1 m) - \cos(c_2 m)][\cos(c_1 n) - \cos(c_2 n)]$, $c_1 = (1 + l/L)\pi/2$, $c_2 = (1 - l/L)\pi/2$, a stands for the amplitude of the excitation term and c represents the wave propagation velocity of the medium.

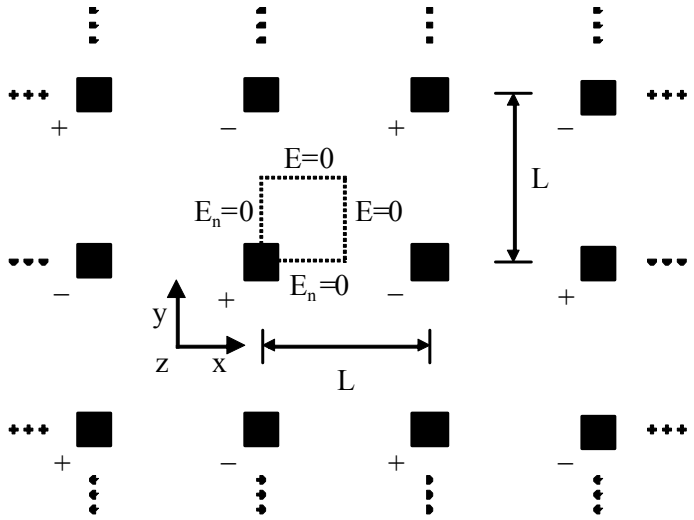

Figure 4. Sketch of the model: square regions of constant electric current densities and discretized domain.

In Fig. 5, the analytical answer and the CDM solution are presented for the time instants $t = 3.5 \cdot 10^{-8} s$ and $t = 5 \cdot 10^{-8} s$. In Fig. 6 the solution computed by the discussed technique and its active dissipative elements in the mesh are depicted, considering or not subcycling. As one can observe, spurious, non-physical oscillations occur in the solution computed by the CDM, whereas, in the new methodology, they are eliminated due to its dissipative features.

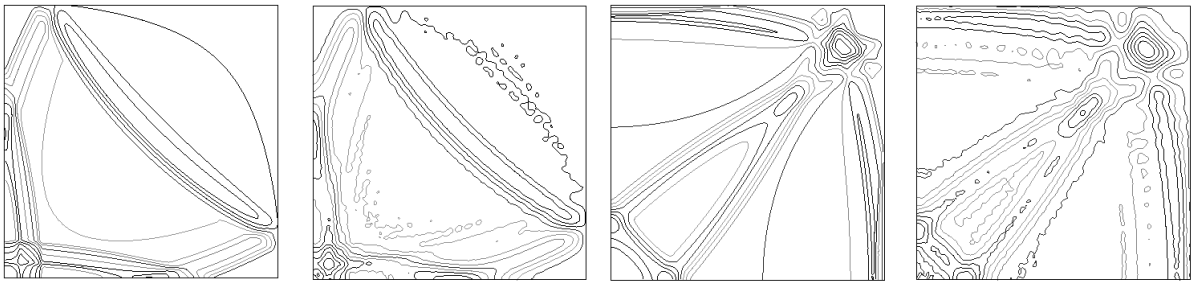

Figure 5. Analytical answer at instants (a) $t = 3.5 \cdot 10^{-8} s$ and (c) $t = 5 \cdot 10^{-8} s$; CDM solution at instants (b) $t = 3.5 \cdot 10^{-8} s$ and (d) $t = 5 \cdot 10^{-8} s$.

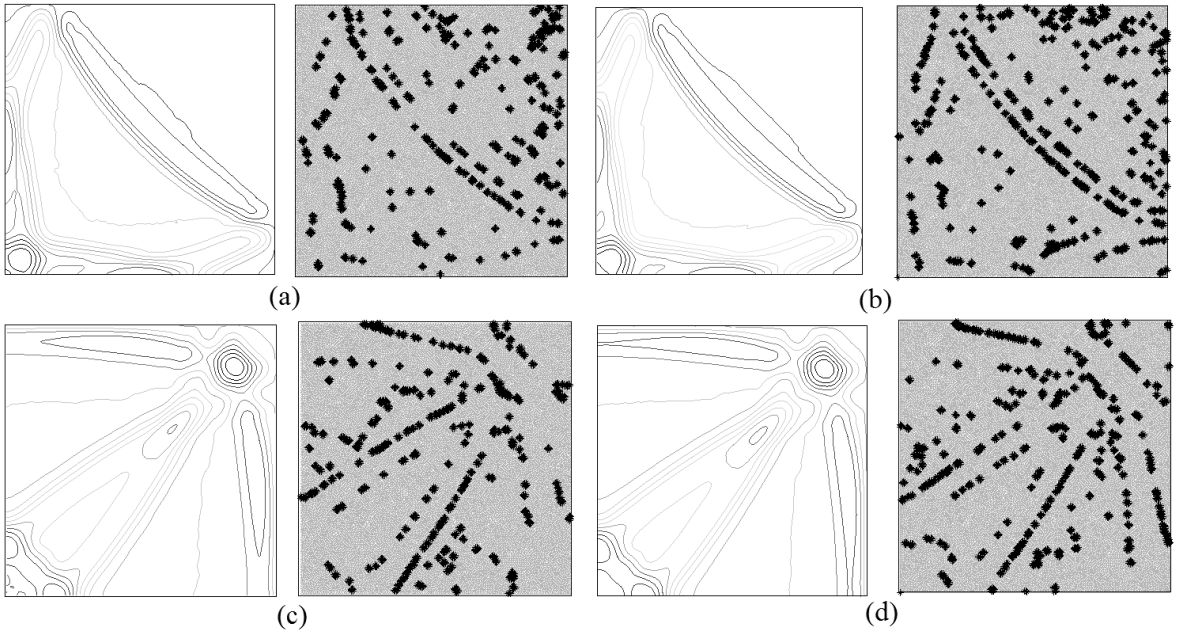

Figure 6. Computed fields and active dissipative elements: (a) with subcycling at $t = 3.5 \cdot 10^{-8} s$; (b) without subcycling at $t = 3.5 \cdot 10^{-8} s$; (c) with subcycling at $t = 5 \cdot 10^{-8} s$; (d) without subcycling at $t = 5 \cdot 10^{-8} s$.

In Fig. 7, time-history results at the middle of the square region (see Fig. 4) are presented, once again illustrating the ability of the discussed technique to properly dissipate the spurious high frequency modes of the model. For this point of analysis, taking into account the adopted discretization, a relative error (L2 norm) of 0.16088 was obtained for the CDM, 0.15858 for the new method without subcycling and 0.13884 for the new method with subcycling (one should observe that by considering appropriate time discretizations for each element, the proposed technique becomes more effective).

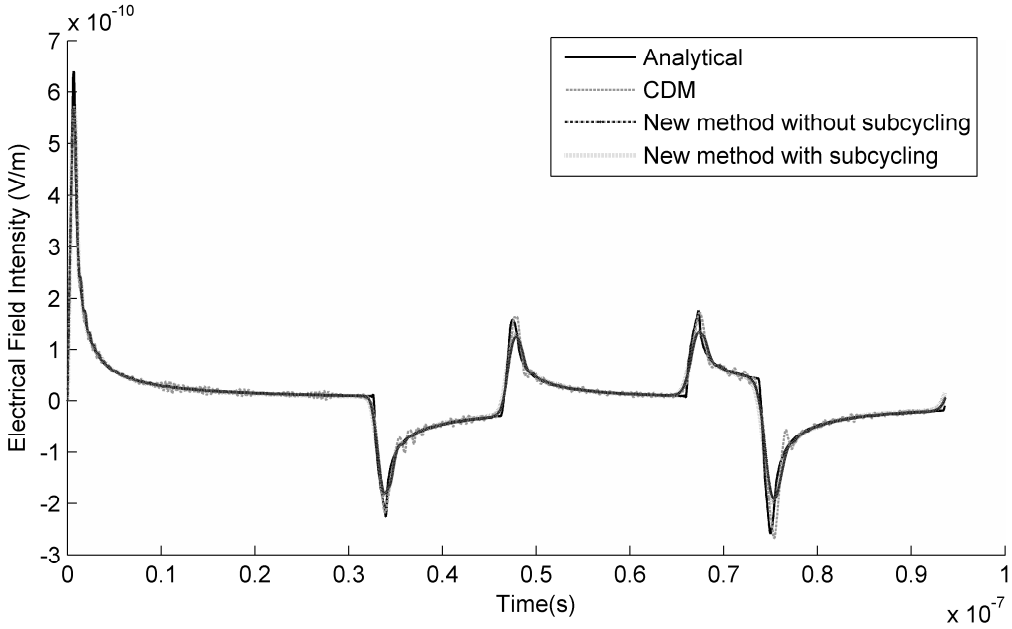

Figure 7. Time-history results at x = L/2 and y = L/2.

6 CONCLUSIONS

An adaptive explicit method to analyze hyperbolic problems is discussed here. The technique is conditionally stable, second-order accurate when $\alpha = 1$ and it allows adaptive dissipation control, being numerical damping introduced into the analysis only when a oscillatory behavior is detected. Thus, spurious high frequency modes can be eliminated without considerable damaging the accuracy of the low modes solution. Additionally, by considering subcycling techniques, the main disadvantage of explicit methods, which is their conditional stability, can be minimized, rendering an effective and efficient methodology. Furthermore, the proposed technique is very easy to implement, standing as a non-iterative single-step approach, which is truly self-starting.

REFERENCES

K. J. Bathe, 1996. *Finite Element Procedures*, Prentice-Hall, Upper Saddle River, New Jersey.

T. Belytschko e R. Mullen, 1977. Explicit integration of structural problems, in: P. Bergen et al., *Finite Elements in Non Linear Mechanics*, vol. 2, pp. 697-720.

M. A. Dokainish and K. Subbaraj, 1989. A Survey of Direct Time-Integration Methods in Computational Structural Dynamics – I. Explicit Methods, *Computer & Structures*, vol. 32, No. 6, 1371-1386, (1989).

G. Großeholz, D. Soares and O. Von Estorff, 2015. A stabilized central difference scheme for dynamic analysis. *International Journal for Numerical Methods in Engineering*, v. 102, p. 1750-1760.

T.J.R. Hugues, 2000. *The Finite Element Method*, Dover Publications INC, New York.

D. Soares, 2014a. An explicit family of time marching procedures with adaptive dissipation control. *International Journal for Numerical Methods in Engineering*, v. 100, p. 165-182.

D. Soares, 2014b. An explicit time marching technique with solution-adaptive time integration parameters, *Technical Report*, UFJF, Juiz de Fora.

D. Soares, 2014c. A simple and effective new family of time marching procedures for dynamics, *Computer Methods in Applied Mechanics and Engineering,* vol. 283, pp. 1138–1166.

D. Soares, 2015. A second-order time-marching procedure with enhanced accuracy. *Computer Modeling in Engineering & Sciences*, vol. 105, no. 5, pp. 341-360.